JCTC Journal of Chemical Theory and Computation

Article

pubs.acs.org/JCTC

Exploring Copper Oxide Cores Using the Projected Hartree–Fock Method

Kousik Samanta,[†] Carlos A. Jiménez-Hoyos,[†] and Gustavo E. Scuseria*[,†,‡]

[†]Department of Chemistry, Rice University, Houston, Texas 77005, United States

[‡]Department of Physics and Astronomy, Rice University, Houston, Texas 77005, United States

ABSTRACT: Coupled binuclear copper oxide cores are present in the active sites of some of the very common metalloenzymes found in most living organisms. The correct theoretical description of the interconversion between the two dominant structural isomers of this core, namely, side-on μ-η^2:η^2-peroxodicopper(II) and bis(μ-oxo)-dicopper(III), is challenging since it requires a method that can provide a balanced description of static and dynamic correlations. We investigate this problem using our recently developed projected Hartree–Fock method (PHF). Here, the spin and complex conjugation symmetries of the trial wave function are deliberately broken and restored in a variation-after-projection scheme. The projected wave function carries good quantum numbers, has multireference character, and accounts for static and some dynamic correlation. Most importantly, the calculations are done at a mean-field computational cost allowing us to address large systems at a modest expense. The interconversion is studied here for the bare $[Cu_2O_2]^{2+}$ core using a variety of projection methods (SUHF, SGHF, KSUHF, KSGHF). The results seem to be on par with much more demanding traditional multireference methods.

1. INTRODUCTION

The metalloproteins containing coupled binuclear (or *type-3*) copper centers are an important part of almost all known living organisms.[1−3] In mollusks and arthropods, for example, the type-3 copper center is located in the active site of hemocyanin that is responsible for oxygen transport and storage.[1] Tyrosinase, an enzyme containing a similar core, catalyzes the monooxygenation of phenol to *o*-diphneol (catechol) and subsequent oxidation of *o*-diphenol to *o*-quinone, a reactive precursor to the formation of the pigment melanin from tyrosine, in a process tied to the protection and healing of wounded tissues in most known organisms.[1,2] Catechol (or polyphenol) oxidase, another ubiquitous metalloenzyme that also contains the type-3 copper core, is responsible for oxidation of *o*-diphenols to corresponding *o*-quinones in a wound-response mechanism similar to tyrosinase.[1,3] The key to the efficiency of these metalloproteins is the ability of the dicopper core to *reversibly* bind to molecular oxygen (O_2) in the corresponding *oxy-forms*, which results in the activation of O_2 for oxygenation/oxidation due to the weakening of the O−O bond.[4]

The oxy-forms of all type-3 metalloproteins have a very similar structure for the $[Cu_2O_2]^{2+}$ core, namely a *side-on* μ-η^2:η^2-peroxodicopper(II) structure, **A** [Figure 1], with each Cu atom being supported by three histidine ligands.[1−4] In this structure, the typical Cu−Cu and O−O bond lengths are ∼3.6 and ∼1.4 Å, and the formal oxidation states of copper and oxygen are Cu(II) and O_2^{2-} (peroxide), respectively. In structure **A**, the unpaired Cu d electrons are antiferromagnetically coupled, and the corresponding metalloenzymes do not respond to electron paramagnetic resonance experiments.[1]

In the past three decades, there has been a large amount of research activity in order to develop synthetic catalysts that mimic the structure and reactivity of the naturally occurring type-3 copper enzymes using various different organic ligands as the support for the core.[5−8] In addition to **A**, a few other stable $[Cu_2O_2]^{2+}$ structures for these synthetic complexes have been identified. Structure **B**, bis(μ-oxo)copper(III) [see Figure 1], is notable for having Cu−Cu and O−O bond lengths of ∼2.8 and ∼2.3 Å, respectively. The oxidation states of copper, Cu(III), and oxygen, O^{2-} (oxide), in **B** are also different from those in **A**.

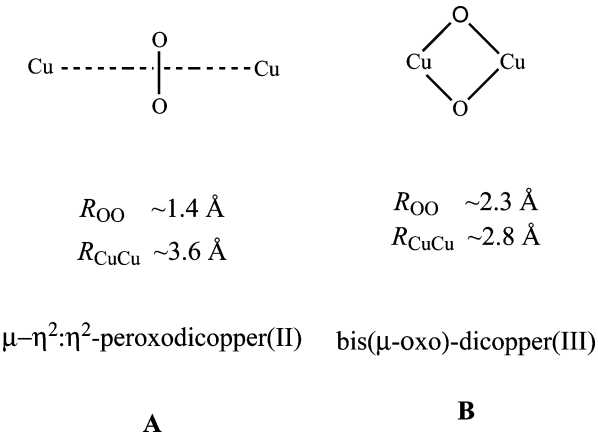

Figure 1. Schematic diagrams of the two dominant structural motifs of the $[Cu_2O_2]^{2+}$ core.

For certain synthetic complexes, structures **A** and **B** are very close in energy with a very low barrier of interconversion, resulting in a rapid equilibrium with each other.[5−8] The equilibrium depends on the nature of the ligands (e.g., denticity, steric bulk, whether N-alkyl, or N-pyridyl donor) as well as the reaction conditions (e.g., concentration, temper-

Special Issue: Berny Schlegel Festschrift

Received: August 4, 2012
Published: September 19, 2012

ature, solvent, counteranion). Moreover, although in oxy-tyrosinase and oxy-catechol oxidase structure **A** is usually considered[1−3] to be the active oxidant where the oxidation of the phenols proceeds via peroxide attack on the arene ring, recent findings[9] about the **A** ⇄ **B** equilibrium have opened up an alternative oxidative mechanistic route, namely O−O bond cleavage before substrate hydroxylation such that **B** acts as the active oxidant. Thus, understanding this equilibrium, as Stack and co-workers noted,[6] is tantamount to "harnessing oxidizing potential of these complexes".

A is a singlet biradical, so in terms of electronic structure theory it presumably has a large amount of static (non-dynamical) correlation originating from the near degeneracy of electronic configurations. In **B**, on the other hand, the correlation seems to be mostly dynamic in nature, originating from small individual contributions of many excited configurations. Thus, in order to study the interconversion **A** ⇄ **B**, one needs a method that can (1) handle such a large system efficiently as well as (2) give a balanced description of static and dynamic correlation as one moves along the isomerization coordinate from one structure to the other. These constraints make the interconversion a very interesting problem from an electronic structure theory point of view.

A review of the theoretical efforts until 2009 for modeling this problem may be found in ref 10. Highly correlated ab initio methods based on a multiconfigurational reference state, e.g., complete/restricted active space self-consistent field method (CASSCF[11−13]/ RASSCF[14]), CASSCF/RASSCF with second-order Møller-Plesset perturbation corrections (CASPT2[11−13]/ RASPT2[14]), and multireference configuration interaction (MR-CI),[15] as well as those based on a single Slater determinant reference state, e.g., completely renormalized coupled cluster (CR-CC)[12,13] and local-pair-natural-orbital coupled cluster (LPNO−CC)[16] methods, have been used to study the problem. Recently, Chan and co-workers have also applied their density matrix renormalization group with canonical transformation method (DMRG-CT) to this problem.[17]

The above methods are usually demanding from a computational viewpoint. For example, multiconfiguration based methods correctly account for static correlation but have unfavorable computational scaling with system size and become impractical for studying large realistic chemical systems.[18−20] For the problem under consideration, one should ideally include in the CASSCF active space at least all the valence orbitals on two Cu (3d and 4s) and two O atoms (2s and 2p) as well as the Cu 4d orbitals in order to avoid a "double-shell" effect (due to the nearly filled Cu 3d orbitals). This results in an active space of 30 orbitals with 28 electrons involving billions of Slater determinants beyond the scope of current CASSCF codes.[10] Methods based on RASSCF,[14] where certain configurations resulting from electron excitations within the active space are excluded, are capable of handling larger (restricted) active spaces (RAS), but the results depend on the choice of the restrictions imposed. Perturbation corrections to CASSCF/RASSCF reference states (CASPT2/RASPT2) bring in additional dynamic correlation; however, if this dynamic correlation is too large one should be cautious about the perturbation considered.[10] The recently developed DMRG methods are an interesting alternative capable of pushing the active space size beyond that of traditional multireference methods.[17,21−23] We here compare our results with CASSCF/RASSCF and DMRG methods. On the other hand, coupled cluster methods (CC) based on a single Slater determinant mostly account for dynamical correlations. In cases where static correlation is dominant (for example, structure **A**), these methods may not be flexible enough to account for all relevant correlations. Completely renormalized coupled cluster methods are an alternative developed to overcome this obstacle.[24] Methods based on density functional theory (DFT) are computationally less demanding, but for the problem under consideration, different functionals, including hybrids, yield very different answers.[11] We do not include them in this study simply because we do not deem them reliable for the problem under consideration.

In this work, we investigate copper oxide cores using our recently developed projected Hartree−Fock method (PHF).[25] PHF recovers a symmetry-adapted wave function from a symmetry-broken trial reference state; symmetries are broken deliberately and then restored in a variation-after-projection scheme (VAP). The projection-after-variation schemes (PAV), unlike VAP, do not yield a variationally optimized solution and are known to compound, rather than fix, the problems associated with the underlying symmetry-broken wave function.[26] VAP is a much more reliable approach in this regard. In this paper, we break and restore the total ($\hat{S}^2$) and z component ($\hat{S}_z$) of spin and the complex conjugation ($\hat{K}$) symmetries. Although PHF is based on a single Slater determinant, it generates a symmetry adapted multireference wave function. The method is capable of describing static as well as some dynamic correlation and has low computational cost comparable to mean-field methods (Hartree−Fock). Moreover, PHF is completely "black box", correlates *all* electrons, and does not necessitate the preselection of an orbital space, be it valence or energy selected. The basis set dependence of PHF is similar to that of CASSCF and is much less severe than CC theory. These attributes make PHF suitable for studying large systems, for example, the copper oxide complexes discussed above.

In closing this introduction, we would like to note that the investigations reported in this paper should be deemed exploratory of the capabilities of our projection methods. The copper oxide **A** ⇄ **B** interconversion is a very challenging problem, and we are interested here in investigating the performance of PHF compared to other sophisticated mainstream techniques.

2. THEORY

Here, we give a brief outline of the theory to establish notation and make the article self-contained. A detailed version of the theory, as well as the derivation of the working equations, has been presented elsewhere.[25,27,28]

If an operator $\hat{\Lambda}$ commutes with the Hamiltonian $\hat{H}$ of the system under consideration, then $\hat{H}$ is said to have the symmetry $\hat{\Lambda}$. For finite systems, eigenfunctions of $\hat{H}$ must be eigenfunctions of $\hat{\Lambda}$ as well. However, an *approximate* wave function obtained, for example, by variationally optimizing a trial wave function may not be an eigenfunction of $\hat{\Lambda}$ unless it is constrained to be so during the variation. The *symmetry-adapted* (approximate) wave function, i.e., the one that is optimized under this symmetry constraint, has lesser variational flexibility, and thus it is usually higher in energy than the *symmetry-broken* one that is optimized without the constraint. In spite of certain severe drawbacks stemming from not being an eigenfunction of $\hat{\Lambda}$, symmetry-broken wave functions give access to a large portion, if not all, of the Hilbert space of the problem even when it is based on a single Slater determinant. This feature is

exploited by our projection technique that filters out, from a symmetry-broken single Slater determinant, a wave function that is not only an eigenfunction of $\hat{\Lambda}$ but also multiconfigurational in nature. We present below an overview of how the symmetry breaking and restoration technique works.

An unrestricted Hartree−Fock (UHF) wave function $|\Phi_{\mathrm{UHF}}\rangle$ is based on a single Slater determinant which, unlike restricted Hartree−Fock (RHF), does not restrict the spatial parts corresponding to up and down spin pairs to be the same; it has *different orbitals for different spins* (DODS), and thus it is not usually an eigenfunction of $\hat{S}^2$.[29,30] In other words, $|\Phi_{\mathrm{UHF}}\rangle$ has the $\hat{S}^2$ symmetry broken, although it is still an eigenfunction of the operator $\hat{S}_z$. Hence, $|\Phi_{\mathrm{UHF}}\rangle$ may be thought of as the following linear combination:

$$|\Phi_{\mathrm{UHF}}\rangle = \sum_s C_{sm}|s;\, m\rangle \tag{1}$$

where $|s;m\rangle$ is an eigenfunction of both $\hat{S}^2$ and $\hat{S}_z$ with $s(s+1)$ and m being the corresponding eigenvalues, and C_{sm} is a mixing coefficient $\langle s;m|\Phi_{\mathrm{UHF}}\rangle$ with $\langle s;m|$ being the *bra* vector corresponding to the *ket* $|s;m\rangle$. The three-dimensional operator[31]

$$\hat{P}^s_{mm'} = |s;\, m\rangle\langle s;\, m'| = \frac{2s+1}{8\pi^2}\int \mathrm{d}\Omega\, [D^s_{mm'}(\Omega)]^*\, \hat{R}(\Omega) \tag{2}$$

may be used to project out a state $|\Psi\rangle = \hat{P}^s_{mm}|\Phi_{\mathrm{UHF}}\rangle$, which is an eigenfunction of $\hat{S}^2$ with eigenvalue $s(s+1)$, from $|\Phi_{\mathrm{UHF}}\rangle$ that is already an eigenfunction of $\hat{S}_z$ with eigenvalue m.[25,27,32] In the above equation, the asterisk indicates complex conjugation,

$$D^s_{mm'}(\Omega) = \langle s;\, m|\hat{R}(\Omega)|s;\, m'\rangle \tag{3}$$

is an element of the Wigner rotation matrix, and

$$\hat{R}(\Omega) = \mathrm{e}^{i\alpha\hat{S}_z}\,\mathrm{e}^{i\beta\hat{S}_y}\,\mathrm{e}^{i\gamma\hat{S}_z} \tag{4}$$

is the corresponding rotation operator defined in terms of the set of Euler angles $\Omega \equiv (\alpha,\beta,\gamma)$ in the three-dimensional spin space. We note in passing that $\hat{P}^s_{mm'}$ is not a true projection operator in a strictly mathematical sense,[25] yet this has no practical consequences in our calculations.

A generalized Hartree−Fock (GHF) wave function

$$|\Phi_{\mathrm{GHF}}\rangle = \sum_{s,m} C_{sm}|s;\, m\rangle \tag{5}$$

is an eigenfunction of neither $\hat{S}^2$ nor $\hat{S}_z$ and clearly has more symmetries broken than UHF.[33,34] In order to obtain a symmetry-restored wave function

$$|\Psi\rangle = \sum_{m'} c_{m'}\hat{P}^s_{mm'}|\Phi_{GHF}\rangle \tag{6}$$

from $|\Phi_{\mathrm{GHF}}\rangle$, one needs to carry out an additional diagonalization to compute the $2s+1$ coefficients $\{c_m\}$ at each cycle so that the energy is minimum and independent of the choice of the quantization axis (see below).

The energy of the spin projected state

$$E[\boldsymbol{\rho}] = \langle\Psi|\hat{H}|\Psi\rangle/\langle\Psi|\Psi\rangle \tag{7}$$

may be expressed as a functional of the one-particle density matrix $\boldsymbol{\rho}$ corresponding to the symmetry-broken state. This enables one to compute an effective Fock matrix $\mathbf{F}$ with

$$\mathrm{F}_{ij} = \partial E[\boldsymbol{\rho}]/\partial\rho_{ij} \tag{8}$$

and devise a self-consistent scheme similar to the regular Hartree−Fock method to variationally minimize $E[\boldsymbol{\rho}]$,[25] where the variational minimum is characterized by

$$[\mathbf{F}, \boldsymbol{\rho}] = 0$$

The spin symmetry restored wave function $|\Psi\rangle$ corresponding to this minimum will be referred to as the SUHF (SGHF) wave function when it is based on a UHF (GHF) trial wave function.

On the other hand, complex conjugation symmetry ($\hat{K}$) may be restored from a $\hat{K}$-symmetry broken wave function $|\Phi\rangle$

$$\hat{K}|\Phi\rangle = |\Phi\rangle^* \neq \mathrm{e}^{i\chi}|\Phi\rangle,\ \chi \in (-\pi,\, \pi] \tag{9}$$

by diagonalizing the Hamiltonian in the basis of $\{\hat{I}|\Phi\rangle,\hat{K}|\Phi\rangle\}$, where $\hat{I}$ (identity operator) and $\hat{K}$ form the complex conjugation group under "multiplication" ($\hat{I}\cdot\hat{I} = \hat{K}\cdot\hat{K} = \hat{I}$, $\hat{I}\cdot\hat{K} = \hat{K}\cdot\hat{I} = \hat{K}$). A KSUHF (KSGHF) wave function is variationally optimized and has $\hat{K}$ as well as $\hat{S}^2$ ($\hat{S}^2$ and $\hat{S}_z$) symmetries restored from a complex UHF (GHF) wave function. The symmetry-broken trial wave function for KSUHF (KSGHF) may be generated, for example, by mixing the highest occupied and lowest unoccupied orbitals of a UHF (GHF) wave function with a complex mixing coefficient. Because complex conjugation symmetry breaking and restoration is a 2×2 configuration interaction between nonorthogonal Slater determinants, we expect it to add mostly dynamical correlation to SUHF and SGHF.

3. RESULTS AND DISCUSSION

We have used the PHF methods, namely SUHF, KSUHF, SGHF, and KSGHF, implemented in a development version of Gaussian[35] to investigate the interconversion of **A** and **B**. The intermediate structures are generated by linearly interpolating the extreme geometries **A** and **B** ("rigid scan") in the same way as described in ref 13.

3.1. Previous Studies. The motivation for this study came from the work of Cramer et al. (CASSCF, CASPT2, and CR-CC),[13] Malmqvist et al. (RASPT2),[14] and Yanai et al. (DMRG methods).[17] The CASSCF calculations involved an active space of 14 orbitals with 16 electrons. In the CASPT2 calculations, which were based on this CASSCF reference state, all the valence and the Cu 3p electrons were correlated. CR-CC results, referred to as CR-CCSD(TQ)$_L$ in ref 13, were computed as CR-CCSD(T)$_L$+{CR-CCSD(TQ)−CR-CCSD(T)} with the 2s and 2p orbitals of O and the 4s and 3d orbitals of Cu correlated explicitly. RASPT2 involved a large active space of 28 orbitals with 24 electrons with the restriction of only allowing a maximum of four holes in RAS1 and a maximum of four particles in RAS3 at a time (RAS1 and RAS3 refer to the fully occupied and fully unoccupied parts of RAS from an RHF point of view). Yanai et al.[17] used three different flavors of DMRG, namely DMRG-CI (no orbital optimization), DMRG-SCF (orbital optimization á la CASSCF), and DMRG-SC-CTSD (DMRG with strongly contracted canonical transformation including only single and double excitations as a means to describe dynamic correlation). All of the DMRG calculations involved an active space of 32 orbitals with 28 electrons. We compare our results with all of the above methods in the following.

3.2. The Model. The rigid scan of the potential energy surface of the $[Cu_2O_2]^{2+}$ core is performed on the bare core and is based on the work of Cramer et al.[13,14] and Yanai et al.[17]

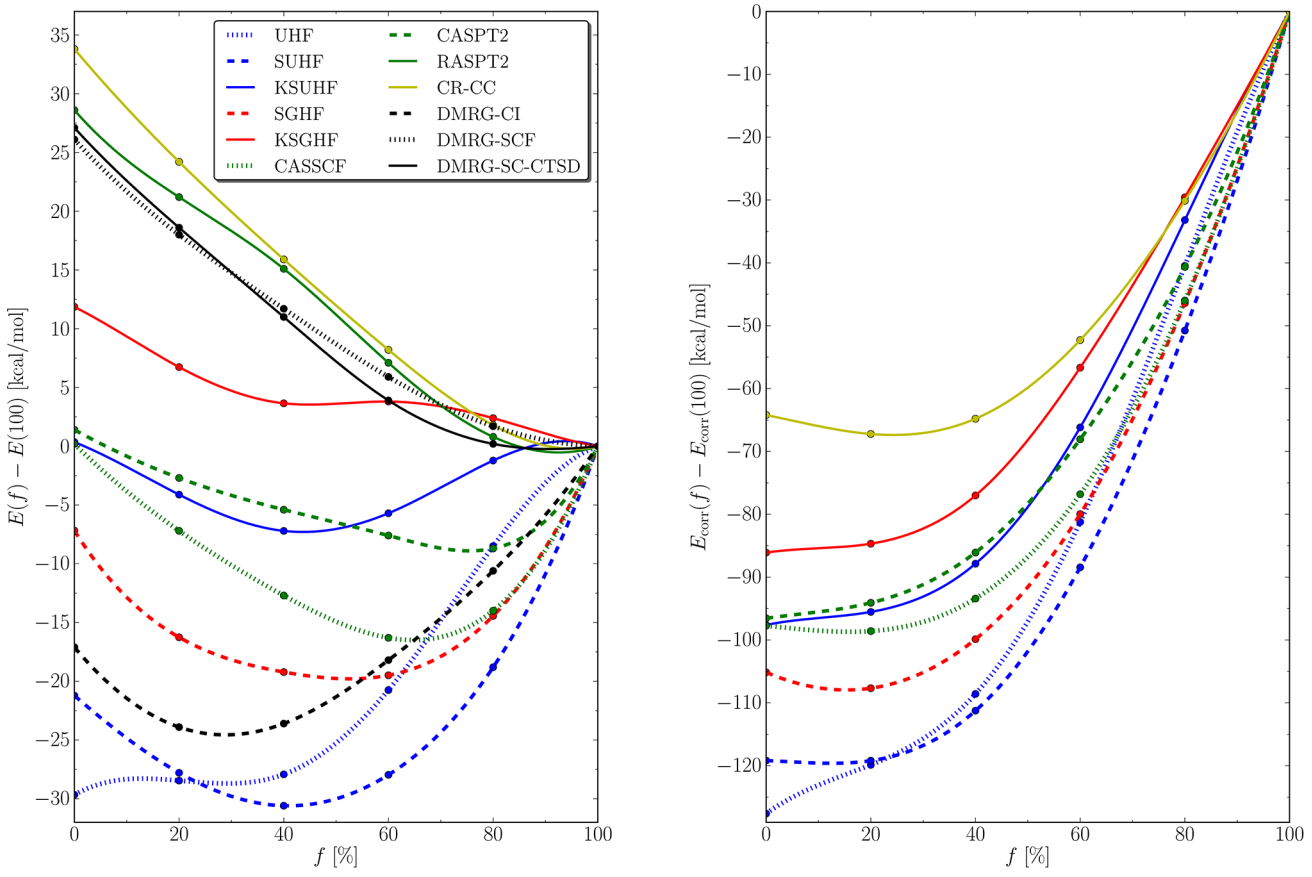

Figure 2. Change in (a) relative total energy and (b) relative correlation energy of $[Cu_2O_2]^{2+}$ along a linear isomerization path from **B**, bis(μ-oxo)-dicopper(III) (f = 0) to **A**, μ-η^2:η^2-peroxodicopper(II) (f = 100). CASSCF, CASPT2, and CR-CC data were extracted from ref 13. RASPT2 and DMRG data were taken from refs 14 and 17, respectively.

As described in ref 13, the geometries of **A** and **B** are chosen to be the "idealized" ones with O−O, Cu−Cu, and Cu−O bond lengths in **A** (**B**) as 1.40 (2.30), 3.60 (2.80), and 1.81 (1.93) Å, respectively. The intermediate geometries are obtained from a simple linear interpolation formula[13]

$$q_i(f) = q_i(0) + \frac{f}{100}[q_i(100) - q_i(0)] \quad (10)$$

where $q_i(f)$ refers to an atomic Cartesian coordinate at a geometry that corresponds to a f% progress from structure **B** (f = 0) toward **A** (f = 100).

3.3. Basis Set. We have used the same basis sets employed in previous works.[13,14,17] These are the quasirelativistic Stuttgart pseudopotential for the 10 core electrons (ECP10MWB) along with the related ECP10MWB basis set [8s7p6d/6s5p3d] for Cu[36] and the all-electron atomic natural orbital (ANO) basis set [14s9p4d/4s3p2d][37] for O. This amounts to a total of 118 basis functions.

3.4. Energetics. The change in relative total energy (E) and relative correlation energy (E_{corr}) obtained from different levels of theory are plotted in Figure 2. Data from the literature, wherever available, are also plotted for comparison. Here and in the following, the relative total (correlation) energies are expressed relative to the total (correlation) energy of **A**. The correlation energy at a given geometry is always measured relative to the RHF total energy at the same geometry. Table 1 lists the relative total energies from the PHF wave functions used in this work.

Table 1. Relative Total Energies of the Isomeric Structures of $[Cu_2O_2]^{2+}$ (in kcal·mol^{-1}) at Various Points along the Linear Isomerization Path from B, Bis(μ-oxo)-dicopper(III) (f = 0) to A, μ-η^2:η^2-Peroxodicopper(II) (f = 100)[a]

f	RHF	UHF	SUHF	KSUHF	SGHF	KSGHF
0	94.4	−29.7	−21.2	0.4	−7.2	11.9
20	88.7	−28.5	−27.8	−4.1	−16.3	6.7
40	78.9	−27.9	−30.6	−7.2	−19.2	3.7
60	59.4	−20.7	−28.0	−5.7	−19.5	3.8
80	31.5	−8.5	−18.8	−1.2	−14.4	2.4

[a]Total energies are computed relative to the total energy of **A**, namely, −541.217338, −541.345890, −541.372117, −541.578786, −541.429628, and −541.640292 hartree at the levels of RHF, UHF, SUHF, KSUHF, SGHF, and KSGHF, respectively.

It is evident from Figure 2a that different methods yield *very* different potential energy curves along the isomerization path. Although the exact answer to this problem is not known, it is currently believed that the methods in the upper portion of Figure 2a (CR-CC, RASPT2, DMRG-SCF, and DMRG-SC-CTSD) are those that yield the most reliable answers. In analyzing the data in Figure 2a, a few general trends may be identified. Several methods (UHF, CASSCF, CASPT2,

dx.doi.org/10.1021/ct300689e | J. Chem. Theory Comput. 2012, 8, 4944−4949

DMRG-CI) indicate that the energies of **B** are comparable to or lower than those of **A**, and their curves pass through a minimum at an intermediate geometry. Of our methods, SUHF and SGHF clearly fall in this category. On the other hand, RASPT2, CR-CC, DMRG-SCF, and DMRG-SC-CTSD calculations place **B** ~26−35 kcal·mol^{-1} above **A**, and there is no minimum along these curves. Interestingly, when we add complex conjugation to our spin projected methods, we see a clear trend in KSUHF and KSGHF for approaching the methods in the upper branch. KSGHF predicts **B** to be above **A** by 11.9 kcal·mol^{-1}. This is shy of the presumably correct answer (~30 kcal·mol^{-1}) but outstanding performance for a method with mean-field (Hartree−Fock) computational cost.

Correlation energies for the structures **A** and **B** are listed in Table 2. Some of the methods in Table 1 (from literature) are not included in Table 2 because relevant data were not available. In case of **A**, KSUHF (SUHF) accounts for about −47 (−82) kcal·mol^{-1} more (less) correlation energy compared to CASSCF. Similarly, KSGHF (SGHF) accounts for about −86 (−46) kcal·mol^{-1} more (less) correlation energy than CASSCF. On the other hand, CASPT2, which presumably accounts for additional dynamic correlation on top of CASSCF, adds about −352 kcal·mol^{-1}, a large amount compared to the active space correlation energy. Regarding CR-CC, ref 13 claims a balanced description of dynamic and static correlation and reported a correlation energy of −581 kcal·mol^{-1} for **A**.

Table 2. Correlation Energies (in kcal·mol^{-1}) for μ-η^2:η^2-Peroxodicopper(II) (A) and Bis(μ-oxo)-dicopper(III) (B) from Different Theoretical Methods

method	A	B
UHF[a]	−80.7	−208.9
SUHF[a]	−97.1	−216.3
KSUHF[a]	−226.8	−324.4
SGHF[a]	−133.2	−238.4
KSGHF[a]	−265.4	−351.5
CASSCF[b]	−179.5	−277.3
CASPT2[b]	−531.5	−628.0
CR-CC[b]	−581.0	−645.2

[a]This work. [b]Computed from the data in ref 13.

Figure 2b shows the change in correlation energy along the isomerization path connecting **A** and **B**. It is evident that all methods predict **B** to be more correlated than **A**. It is also interesting to note that the plot for KSUHF lies in between those for CASSCF and CASPT2. This is a clear indication that our simplest spin projection method, KSUHF, is comparable to the computationally much more demanding multireference methods in accounting for relevant correlations. The change in correlation energy for SUHF along the isomerization path is relatively larger than those for the other methods, but it still follows the same trend. The change in KSGHF correlation energy is, however, much closer to CR-CC than any of the other methods discussed here. In our interpretation, SGHF builds static correlation in a larger space than SUHF via noncollinear determinants (the latter does so collinearly), whereas "K" seems to add mostly dynamic correlation.

3.5. Wave Function Analysis. Natural spin orbital occupations (n_i, for spin orbital i, $0 < n_i < 1$) are often considered good indicators of multireference character of the underlying wave function. For all the PHF methods considered here, we find at least four (eight) spin orbitals with occupations in the 0.3 to 0.8 range for **A** (**B**). This clearly indicates that the corresponding wave functions are multireference in nature.

A quantitative measure of multireference character (or *entanglement*) is the symmetrized von Neumann entropy[38]

$$\mathcal{S} = -\frac{1}{2}\sum_i [n_i \ln n_i + (1 - n_i)\ln(1 - n_i)] \quad (11)$$

$\mathcal{S}$ is zero for a single determinant wave function that has an idempotent one-particle density matrix (i.e., $n_i = 0$ or 1 for all i). We use $(\mathcal{S}/\mathcal{S}_{max}) \times 10^2$, the percentage of maximum von Neumann entropy captured by a wave function, to gauge its multireference character. The maximum von Neumann entropy ($\mathcal{S}_{max}$) is obtained in the fully entangled case (all up and down spins evenly distributed among all up and down spin orbitals, respectively). Figure 3 shows $\mathcal{S}/\mathcal{S}_{max}$ along the isomerization path. The entanglement entropy obtained here is indicative of strong multireference character.

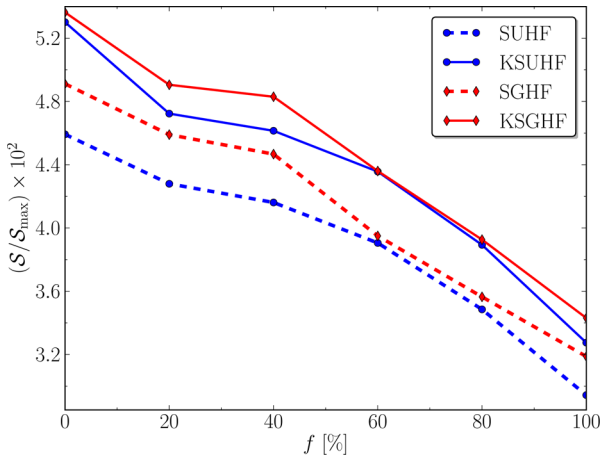

Figure 3. Change in the von Neumann entropy ($\mathcal{S}$) along the linear isomerization path for $[Cu_2O_2]^{2+}$ from **B**, bis(μ-oxo)-dicopper(III) (f = 0), to **A**, μ-η^2:η^2-peroxodicopper(II) (f = 100), where the path is characterized by the conversion percentage (f).

It is commonly stated in the literature (see for example ref 10) that because of the antiferromagnetic coupling between the unpaired Cu 3d orbitals, **A** requires a multireference wave function comprising *at least* the configurations with variable occupations in the (mostly) Cu-type orbitals. We do not disagree with this statement. However, the PHF wave functions for **A** include determinants with variable occupations in Cu-type *as well as* O-type orbitals. Thus, the fact that Figure 3 indicates a higher multireference character for **B** compared to **A** seems to stem from capturing the *overall* multireference character—not *just* that in the Cu-type orbitals.

4. CONCLUSIONS

The $[Cu_2O_2]^{2+}$ core, paradigmatic of current challenges posed to electronic structure methods, have been studied with our recently developed SUHF, KSUHF, SGHF, and KSGHF wave functions. In these methods, total spin ($\hat{S}^2$) and complex conjugation ($\hat{K}$) symmetries are deliberately broken in the single reference determinant and restored in a variation-after-projection scheme that yields a multireference wave function.

SUHF, SGHF, and KSUHF relative energies along a linear isomerization path connecting the **A** and **B** structures of the bare $[Cu_2O_2]^{2+}$ core are very similar to those obtained from

CASSCF and CASPT2. The restoration of complex conjugation and three-dimensional spin projection using KSGHF makes the change in relative energies follow the same trend as the more accurate methods, namely CR-CC, RASPT2, and DMRG-SCF/DMRG-CTSD.

Analysis of our wave functions reveals that both the **A** and **B** structures have strong multireference character. Residual correlations missing in our methods cannot change the qualitative nature of this conclusion. Nevertheless, we would like to emphasize in closing that we cannot deem the calculations reported in this paper quantitatively conclusive. More work is needed to address the challenge of accurately accounting for residual correlations not present in our projection methods. In any event, given their low (mean-field) computational cost and the qualitative agreement with CASSCF and CASPT2 results, we deem our results highly encouraging.

AUTHOR INFORMATION

Corresponding Author

*E-mail: guscus@rice.edu.

Notes

The authors declare no competing financial interest.

ACKNOWLEDGMENTS

This work was supported by the Department of Energy, Office of Basic Energy Sciences, Grant No. DE-FG02-09ER16053 and the Welch Foundation (C-0036).

REFERENCES

(1) Solomon, E. I.; Sundaram, U. M.; Machonkin, T. E. *Chem. Rev.* **1996**, *96*, 2563−2606.
(2) Kitajima, N.; Moro-oka, Y. *Chem. Rev.* **1994**, *94*, 737−757.
(3) Gerdemann, C.; Eicken, C.; Krebs, B. *Acc. Chem. Res.* **2002**, *35*, 183−191.
(4) Citek, C.; Lyons, C. T.; Wasinger, E. C.; Stack, T. D. P. *Nat. Chem.* **2012**, *4*, 317−322.
(5) Jung, B.; Karlin, K. D.; Zuberbühler, A. D. *J. Am. Chem. Soc.* **1996**, *118*, 3763−3764.
(6) Mahadevan, V.; Henson, M. J.; Solomon, E. I.; Stack, T. D. P. *J. Am. Chem. Soc.* **2000**, *122*, 10249−10250.
(7) Mirica, L. M.; Ottenwaelder, X.; Stack, T. D. P. *Chem. Rev.* **2004**, *104*, 1013−1046.
(8) Hatcher, L. Q.; Karlin, K. D. *Adv. Inorg. Chem.* **2006**, *58*, 131−184.
(9) Mirica, L.; Vance, M.; Rudd, D.; Hedman, B.; Hodgson, K.; Solomon, E.; Stack, T. *Science* **2005**, *308*, 1890−1892.
(10) Gherman, B. F.; Cramer, C. J. *Coord. Chem. Rev.* **2009**, *253*, 723−753.
(11) Flock, M.; Pierloot, K. *J. Phys. Chem. A* **1999**, *2*, 95−102.
(12) Cramer, C.; Kinal, A.; Włoch, M.; Piecuch, P.; Gagliardi, L. *J. Phys. Chem. A* **2006**, *110*, 11557−68.
(13) Cramer, C. J.; Włoch, M.; Piecuch, P.; Puzzarini, C.; Gagliardi, L. *J. Phys. Chem. A* **2006**, *110*, 1991−2004.
(14) Malmqvist, P. A.; Pierloot, K.; Shahi, A. R. M.; Cramer, C. J.; Gagliardi, L. *J. Chem. Phys.* **2008**, *128*, 204109.
(15) Rode, M. F.; Werner, H.-J. *Theor. Chem. Acc.* **2005**, *114*, 309−317.
(16) Liakos, D.; Neese, F. *J. Chem. Theory Comput.* **2011**, *7*, 1511−1523.
(17) Yanai, T.; Kurashige, Y.; Neuscamman, E.; Chan, G. K. *J. Chem. Phys.* **2010**, *132*, 024105.
(18) Roos, B. O. *Adv. Chem. Phys.* **1987**, *69*, 399.
(19) Schmidt, M. W.; Gordon, M. S. *Annu. Rev. Phys. Chem.* **1998**, *49*, 233−266.
(20) Olsen, J. *Int. J. Quantum Chem.* **2011**, *111*, 3267−3272.
(21) Chan, G. K.; Kállay, M.; Gauss, J. *J. Chem. Phys.* **2004**, *121*, 6110.
(22) Ghosh, D.; Hachmann, J.; Yanai, T.; Chan, G. K. *J. Chem. Phys.* **2008**, *128*, 144117.
(23) Kurashige, Y.; Yanai, T. *J. Chem. Phys.* **2009**, *130*, 234114.
(24) Piecuch, P.; Włoch, M. *J. Chem. Phys.* **2005**, *123*, 224105.
(25) Jiménez-Hoyos, C. A.; Henderson, T. M.; Tsuchimochi, T.; Scuseria, G. E. *J. Chem. Phys.* **2012**, *136*, 164109.
(26) Schlegel, H. B. *J. Chem. Phys.* **1986**, *84*, 4530.
(27) Scuseria, G. E.; Jiménez-Hoyos, C. A.; Henderson, T. M.; Samanta, K.; Ellis, J. K. *J. Chem. Phys.* **2011**, *135*, 124108.
(28) Rodríguez-Guzmán, R.; Schmid, K. W.; Jiménez-Hoyos, C. A.; Scuseria, G. E. *Phys. Rev. B* **2012**, *85*, 245130.
(29) Pople, J. A.; Nesbet, R. K. *J. Chem. Phys.* **1954**, *22*, 571−572.
(30) Szabo, A.; Ostlund, N. S. *Modern Quantum Chemistry*; Dover Publications: New York, 1996.
(31) Percus, J. K.; Rotenberg, A. *J. Math. Phys.* **1962**, *3*, 928−932.
(32) Schmid, K.; Dahm, T.; Margueron, J.; Müther, H. *Phys. Rev. B* **2005**, *72*, 1−15.
(33) Löwdin, P.-O.; Mayer, I. *Adv. Quantum Chem.* **1992**, *24*, 79−114.
(34) Jiménez-Hoyos, C. A.; Henderson, T. M.; Scuseria, G. E. *J. Chem. Theory Comput.* **2011**, *7*, 2667−2674.
(35) Frisch, M. J.; Trucks, G. W.; Schlegel, H. B.; Scuseria, G. E.; Robb, M. A.; Cheeseman, J. R.; Scalmani, G.; Barone, V.; Mennucci, B.; Petersson, G. A.; Nakatsuji, H.; Caricato, M.; Li, X.; Hratchian, H. P.; Izmaylov, A. F.; Bloino, J.; Zheng, G.; Sonnenberg, J. L.; Hada, M.; Ehara, M.; Toyota, K.; Fukuda, R.; Hasegawa, J.; Ishida, M.; Nakajima, T.; Honda, Y.; Kitao, O.; Nakai, H.; Vreven, T.; Montgomery, J. A., Jr.; Peralta, J. E.; Ogliaro, F.; Bearpark, M.; Heyd, J. J.; Brothers, E.; Kudin, K. N.; Staroverov, V. N.; Kobayashi, R.; Normand, J.; Raghavachari, K.; Rendell, A.; Burant, J. C.; Iyengar, S. S.; Tomasi, J.; Cossi, M.; Rega, N.; Millam, J. M.; Klene, M.; Knox, J. E.; Cross, J. B.; Bakken, V.; Adamo, C.; Jaramillo, J.; Gomperts, R.; Stratmann, R. E.; Yazyev, O.; Austin, A. J.; Cammi, R.; Pomelli, C.; Ochterski, J. W.; Martin, R. L.; Morokuma, K.; Zakrzewski, V. G.; Voth, G. A.; Salvador, P.; Dannenberg, J. J.; Dapprich, S.; Daniels, A. D.; Farkas, Ö.; Foresman, J. B.; Ortiz, J. V.; Cioslowski, J.; Fox, D. J. *Gaussian 09*, Revision H.1; Gaussian Inc.: Wallingford, CT, 2009.
(36) Dolg, M.; Wedig, U.; Stoll, H.; Preuss, H. *J. Chem. Phys.* **1987**, *86*, 866−872.
(37) Pierloot, K.; Dumez, B.; Widmark, P.; Roos, B. O. *Theor. Chem. Acc.* **1995**, *90*, 87−114.
(38) Peschel, I. *Braz. J. Phys.* **2012**, *42*, 267−291.